Research Square

Preprints are preliminary reports that have not undergone peer review.
They should not be considered conclusive, used to inform clinical practice,
or referenced by the media as validated information.

Impact of Different Multi-Source Vertical DEM Accuracy on Deformation Estimation in the Pasuruan Fault Zone using Development of Decomposition Calculation LOS InSAR, Azimuth Tracking Offset, and GPS

Saiyidinal Fikri
Institut Teknologi Sepuluh Nopember
Ira Mutiara Anjasmara
i.anjasmara@its.ac.id

Institut Teknologi Sepuluh Nopember
Mokhamad Nur Cahyadi
Institut Teknologi Sepuluh Nopember
Putra Maulida
Institut Teknologi Sepuluh Nopember

Research Article

Keywords: DEM, PS-InSAR, SBAS, Azimuth Tracking Offset, GPS, Decomposition

Posted Date: February 26th, 2026

DOI: https://doi.org/10.21203/rs.3.rs-8906245/v1

License: This work is licensed under a Creative Commons Attribution 4.0 International License.
Read Full License

Additional Declarations: No competing interests reported.

Version of Record: A version of this preprint was published at Earth Science Informatics on June 19th, 2026. See the published version at https://doi.org/10.1007/s12145-026-02168-w.

Impact of Different Multi-Source Vertical DEM Accuracy on Deformation Estimation in the Pasuruan Fault Zone using Development of Decomposition Calculation LOS InSAR, Azimuth Tracking Offset, and GPS

Saiyidinal Fikri[1,2], Ira Mutiara Anjasmara[1*], Mokhamad Nur Cahyadi[1], Putra Maulida[1]

[1*]Department of Geomatics Engineering, Institut Teknologi Sepuluh Nopember, Sukolilo Campus, Surabaya, 60111, Indonesia.
[2]Geodesy Undergraduate Program, Institut Teknologi Padang, Gajah Mada, Padang, 25122, Indonesia.

*Corresponding author(s). E-mail(s): i.anjasmara@its.ac.id;
Contributing authors: saiyidinal.fikri@gmail.com;
cahyadi@geodesy.its.ac.id; putra@its.ac.id;

Abstract

The main challenge in analyzing fault activity using geodetic methods is estimating accurate 3D components. This study presents a combination of several geodetic methods, namely LOS InSAR, Azimuth Tracking Offset, and GPS Station Ina-CORS, in decomposition calculations to obtain good horizontal and vertical components. To ensure accurate estimation of deformation results from LOS InSAR, this study analyzed several DEMs that are suitable for topographic phase correction, followed by testing the vertical accuracy of each DEM used in the processing. In addition, the combination of PS-InSAR and SBAS aims to obtain adequate accuracy and a number of points in describing deformation in LOS. Due to the insensitivity of LOS InSAR results in the azimuth direction, this study uses the azimuth tracking offset method to obtain estimates of deformation movement in the azimuth direction. The Ina-CORS Station's GPS shift velocity data for the ve and vn components are also presented in this study. By integrating all data processing outcomes into a single equation, 3D decomposition produced the final deformation or shift velocity estimations that are

displayed. The three primary components of the analysis, VN and VU, are the outcomes. The decomposition model developed can handle the difficulty of portraying geodynamic activity happening in fault zones, especially the Pasuruan fault, according to the results of this decomposition calculation.

Keywords: DEM, PS-InSAR, SBAS, Azimuth Tracking Offset, GPS, Decomposition

1 Introduction

East Java is situated in the convergence zone of the Indo-Australian and Eurasian plates, with the former moving 6–7 cm per year towards the latter. This interaction creates a southern fault line and the Sunda Trench (Clements et al. 2009). The Baribis-Kendeng fault system remains active and continues to change (Koulali et al. 2017). The Kendeng thrust fault, also known as the Java Back-Arc Thrust, is a long geological feature extending from West Java to East Java (Widjajanti et al. 2020). Studies of the Earth's crust have found that shallow faults are present along the Pasuruan Fault, although the extent of deformation remains undisclosed. According to seismological research, earthquakes in the Pasuruan fault area result from normal faulting (Marliyani et al. 2019). The Ina-CORS network is monitoring the changes in the Earth's crust in East Java. However, due to the low number of stations in this area, both the resolution and the network's capability in the most active fault zones are weakened (Maulida et al. 2023; Purwaningsih et al. 2022). Synthetic Aperture Radar (SAR) is a solution to these challenges facing geodesy by providing broad coverage, continuous data collection, and improved detection.

SAR interferometry is a technique used to detect changes on Earth's surface across different types of terrain. The Persistent Scatterer Interferometric Synthetic Aperture Radar (PS-InSAR) technique (Ferretti et al. 2001) identifies persistent stable objects that reflect radar signals. The Small Baseline Area Subset (SBAS) method (Berardino et al. 2002) determines changes over time from pairs of images that are close in both temporal and spatial terms. Both approaches are effective at reducing atmospheric impacts, and their combined use results in higher phase accuracy and pixel density. The combination of these methods is a powerful tool for addressing problems in high mountains and dense forests (Bayer et al. 2017), as they are not only compatible with each other but also expected to exhibit synergistic effects on pixel generation (Fikri et al. 2024). Unfortunately, in a complex landscape and a thick forest where radar signals are weak or absent, both methods can only provide rough estimates of deformation data. Typically, steep and heavily forested areas have fewer detectable sites; thus, confirmation is more difficult (Yan et al. 2024). Moreover, the C-band of Sentinel-1 is not a good penetrator of the densest canopy parts, which means deformation measurements may not be as accurate (Jiang and Guarnieri 2020).

Digital Elevation Model (DEM) refers to a 3D representation of the Earth's surface based on a 2D grid, where each cell contains a vertical value (Guth et al. 2021). DEMs are also necessary for topographic correction in PS-InSAR and SBAS processing. The Shuttle Radar Topography Mission (SRTM-1, 30 m) provides broad-area coverage with

a vertical precision approximately of 16 m (Farr and Kobrick 2000). On the other hand, the Copernicus DEM (30 m) gives better vertical accuracy (less than 4 m) (Airbus Defence and Space 2022). The Indonesian National DEM (DEMNAS) has a resolution of 8 m, which may provide more detail, but its vertical accuracy still requires additional field checks (Fikri et al. 2024). Differences among DEM sources can cause phase to change by a few radians per meter, leading to percent-level phase unwrapping errors and corresponding changes in deformation estimates (Bayer et al. 2017; Liu et al. 2023). As part of this research, a vertical accuracy comparison of SRTM-1, Copernicus, and DEMNAS for Pasuruan is being conducted, as field validation is lacking in the area. The accuracy verification is performed using the root mean square error (RMSE) between DEM elevations and field measurements and the Linear Error (LE) at a 90% confidence level.

The research involves comparing DEM data obtained from various sources to evaluate the extent of differences and their influence on PS-InSAR and SBAS results. To confirm these differences, vertical accuracy tests are conducted near the Pasuruan fault. Changes in the Earth's surface have been studied over the period from 2017 to 2024 using an integrated approach that combines PS-InSAR and SBAS methods. Information on horizontal component east–west (Ve) and north–south velocity (Vn) measurements is supported by East Java Ina-CORS (Indonesia Continuously Operating Reference Stations) stations (Maulida et al. 2023). To improve InSAR accuracy, the azimuth tracking offset observation method is used to measure north-south deformation (Chae et al. 2019; Huang et al. 2020; Peng et al. 2022). The results are then processed in a decomposition stage developed in this study, which produces three-dimensional components (VU, VE, and VN) (Hayati et al. 2023; Zhou et al. 2021) using parameter result LOS InSAR, azimuth tracking offset, and component GPS (Ve and Vn).

2 Data, Processing, and Methods

2.1 DEM and Sentinel-1 Data

This study examines three elevation models: DEMNAS, SRTM-1, and Copernicus DEM. These models are used to correct errors when measuring changes in land. Liu (Liu and Wang 2023) found that each model records these changes in its own way during the correction process. After introducing the elevation models, highlight key features and uses for each in a similar way. SRTM-1 is a worldwide map showing land height (30 meters between data points, error about 16 meters), used by NASA and NIMA, covering most of Earth (Farr and Kobrick 2000). Copernicus DEM is also global (data points every 30 meters, error about 4 meters), built by joining data from radar and three other satellite sources. It mainly helps track changes in ground level by a method called InSAR (Airbus Defence and Space 2022). IFSAR data (5 m resolution), TERRASAR-X (5 m resampling resolution from the original 5-10 m resolution), and ALOS PALSAR (11.25 m resolution) are among the data sources used to create DEMNAS. Mass point data used to create the Indonesian Land Map in Indonesia (RBI) (Julzarika and Harintaka 2019).

Table 1 Information of digital elevation models (DEMs) used in this study. HR = horizontal resolution; H-datum = horizontal datum; V-datum = vertical datum; V-acc = vertical accuracy.

DEM	HR (m)	H-datum	V-datum	V-acc (m)
SRTM-1	30	WGS84	EGM96	±16[a]
Copernicus	30	WGS84	EGM2008	±4[a]
DEMNAS	7.5	WGS84	EGM2008	Unknown[b]

Source references: SRTM-1 (Farr and Kobrick 2000); Copernicus DEM (Airbus Defence and Space 2022); DEMNAS (Badan Informasi Geospasial 2018).
[a] Vertical accuracy values are reported as absolute height accuracy under nominal conditions.
[b] The official vertical accuracy of DEMNAS is not explicitly stated in the referenced documentation.

This investigation analyzes Sentinel-1 data from 2017 to 2024 to ensure sufficient temporal resolution for tracking the slow deformation dynamics of the Pasuruan fault. To quantify deformation in the line-of-sight (LOS) direction, we combined the PS-InSAR and SBAS methods, enabling cross-validation of DEM vertical accuracy and assessing its influence on deformation measurements. For deformation monitoring on the Pasuruan fault, 149 ascending and 79 descending scenes were selected.

2.2 Study Area

The study area encompasses the Pasuruan Fault and its surrounding region in Pasuruan Regency, East Java, Indonesia. The area extends from 112°59′24″ E to 113°15′25″ E and from 7°29′31″ S to 7°45′14″ S.The research area has a lowland to low hill morphology with land use dominated by agriculture, settlements, and industrial areas. The variation in elevation within the DEM utilized in this research highlights the necessity for testing vertical accuracy. This is connected to the phase unwrapping process that occurs later. Therefore, by verifying the vertical accuracy of the three DEM datasets, the precision of deformation monitoring can be enhanced.

2.3 Methods

2.3.1 DEM Accuracy Testing

The degree of congruence between the geographical locations depicted on the base map and the real sites in the field is what determines how accurate base maps are. Horizontal and vertical accuracy tests are used to evaluate this precision (Badan Standarisasi Nasional 2019). The conformity between a point's height or elevation on a map and its actual elevation in the field is measured by vertical accuracy. Three DEMs were tested for vertical accuracy by comparing each model's elevation values with field reference data in the form of high-precision RTK readings. According to the minimal quadrant distribution criteria as stated, a total of 24 control sites were dispersed over the study region. Four quadrants were created from the region to be tested, and each quadrant should include at least 20% of the total number of test points (n). Test locations were separated by at least 10% of the diagonal distance (Badan Standarisasi Nasional 2019) (Fig. 1). For maps that show elevation data, such as contours or elevation models, this precision is crucial. Testing is carried out by comparing the elevation values of

control points measured in the field with the same elevation values on the map. The test results are expressed in height units, and RMSE is used as an indicator of vertical accuracy.



Fig. 1 Distribution of vertical accuracy testing points

Each point was observed using the Real Time Kinematic (RTK) method with a "fixed" solution status, a minimum measurement duration of 15 minutes, and good accuracy and precision (Dabove and Di Pietra 2019). To guarantee compatibility with the DEM reference system, the observation results were transformed into a consistent projection system and vertical datum (Susetyo 2023). Each DEM's elevation values were spatially extracted at the test points' coordinates. For every point, the elevation difference (Δh) between the RTK and the DEM was computed. Three vertical accuracy statistical parameters were derived from this difference: the mean error, which characterizes the systematic bias in relation to the reference elevation; the root mean square error (RMSE), which shows the average magnitude of the quadratic error; and the linear error at a 90% confidence level, where the standard deviation of this elevation difference follows a particular equation.

$$\mathrm{RMSE}_z = \sqrt{\frac{1}{n}\sum_{i=1}^{n}\left(z_i^{\mathrm{data}} - z_i^{\mathrm{check}}\right)^2} \tag{1}$$

$$\mathrm{Accuracy}_z = 1.6499\,\mathrm{RMSE}_z \tag{2}$$

2.3.2 PS-InSAR and SBAS

PS-InSAR (Fig. 2 A and B) and SBAS (Fig. 2 C and D) to evaluate their deformation measurement precision and dependability. While each approach is most effective when used with a different kind of scatterer, combining them enables more thorough and dependable monitoring (Hooper 2008). The number and consistency of deformation measurements increase when both approaches are combined, especially when the data contain various scatterer pixel types. According to Fikri (Fikri et al. 2024), combining the two methods yields a higher density of deformation points. The reason is that PS-InSAR provides stable, long-term phase and high coherence, while SBAS is sensitive to short-term changes and offers good temporal resolution. By using the phase and amplitude values of pixels identified by both methods, the researchers can obtain more precise and reliable deformation estimates (Zhang et al. 2023).

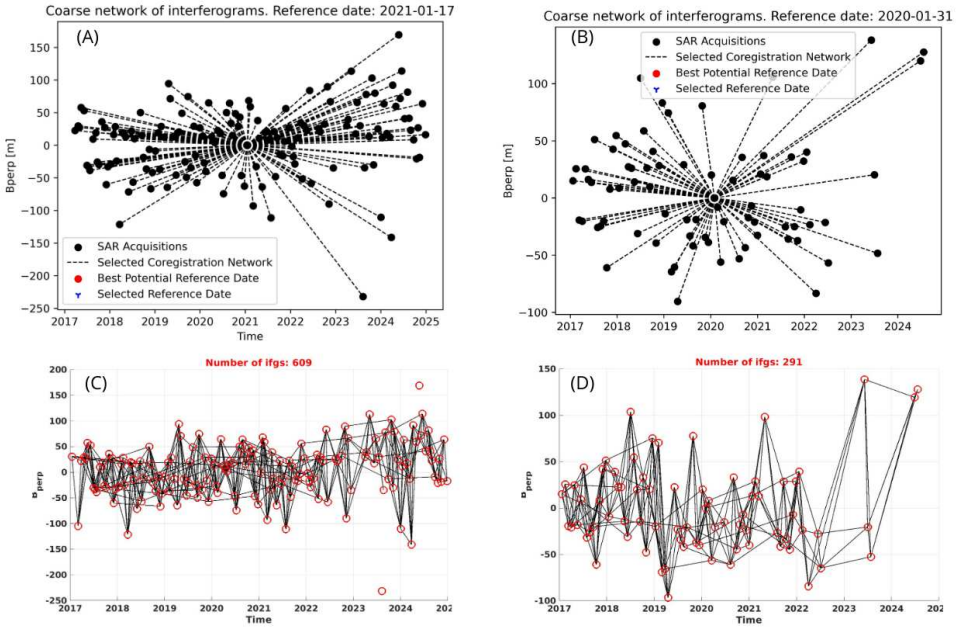


Fig. 2 Visualization of PS-InSAR and SBAS interferogram networks for the period 2017 to 2024, Ascending (A and C) and Descending (B and D).

When PS-InSAR and SBAS technologies are combined, more deformation points are detected during data processing. Additionally, the signal-to-noise ratio (SNR) increases, thereby improving phase unwrapping effectiveness and deformation estimate accuracy (Hooper 2008). Bouraoui (2013) shows that combining the two approaches results in a 40% increase in pixel coverage. This shows that combining both approaches yields better outcomes than using just one. According to Zhang et al. (2023), the

combined approach increased the density of observation the point density in the deformation area increased from 711 to 2,760 points km^2. Additionally, Zhang et al. (2023) stressed that combining PS-InSAR and SBAS preserves the temporal consistency and reliability of deformation measurements while increasing the number of observation points.

2.3.3 Azimuth Tracking Offset

The azimuthal motion of the scene is one of the most challenging tasks to derive from Sentinel-1 SAR images, because changes in azimuthal direction are minimal most of the time and fall within the sensor's spatial resolution, making signal isolation difficult. Thus, to overcome the challenges, the azimuth-tracking offset was determined via cross-correlation of image pairs in this study. According to Ma et al. (2023), comparing each analysis window between the reference and secondary scenes and calculating displacement vectors along the azimuth direction is a good example. Qin et al. (2018) has even gone further to assert that the window size and patch parameters are the most influential factors in determining the trustworthiness of azimuth offset measurements. With approximately 5 and 20 meters of sensor range and corresponding azimuth resolutions, minor ground movements due to the fault may not be precisely captured. Therefore, sub-pixel accuracy will be achieved by incorporating a highly sophisticated Normalized Cross-Correlation (NCC) algorithm. This technique has been tested and found effective in various fields. For example, Sartika et al. (2019) noted that when NCC is used for geometric correction of high-resolution imagery, significant improvements in mapping results are possible. In addition, Fang et al. (2020) demonstrated that sub-pixel accuracy algorithms remain highly effective when applied to Sentinel-1 data, especially for azimuth-oriented motion tracking in glacier studies.

2.3.4 Decomposition

Data on deformation, acquired from the LOS combination of different deformation directions, are included in the InSAR velocity. In a decomposition approach, the east-west and vertical motion components are reversed for each pixel, with ascending and descending geometric information provided. To increase the accuracy of the analysis, this method takes into consideration the angle of incidence of the satellite, following the methodology outlined by Wright et al. (2004), Hussain et al. (2016), and Weiss et al. (2020). The purpose of this method is to combine deformation information from satellite trajectories that are ascending and descending. Due to its geometric restrictions in LOS mode, InSAR is more sensitive to vertical deformation (VU) than east-west horizontal (VE) and north-south (VN) deformation Hayati et al. (2023). In this study, we refer to the research by Zhou et al. (2021) and Hayati et al. (2023) in constructing a decomposition calculation model, by adding the E and N components observed by the Ina-CORS GPS station spread across East Java into the 3D decomposition matrix.

$$\begin{bmatrix} \cos\theta_{\text{inc,asc}} & -\sin\theta_{\text{inc,asc}}\sin\alpha_{\text{h,asc}} & -\sin\theta_{\text{inc,asc}}\cos\alpha_{\text{h,asc}} \\ \cos\theta_{\text{inc,dsc}} & -\sin\theta_{\text{inc,dsc}}\sin\alpha_{\text{h,dsc}} & -\sin\theta_{\text{inc,dsc}}\cos\alpha_{\text{h,dsc}} \\ 0 & \sin\alpha_{\text{h,asc}} & \cos\alpha_{\text{h,asc}} \\ 0 & \sin\alpha_{\text{h,dsc}} & \cos\alpha_{\text{h,dsc}} \\ 0 & 1 & 0 \\ 0 & 0 & 1 \end{bmatrix} \begin{bmatrix} V_U \\ V_E \\ V_N \end{bmatrix} = \begin{bmatrix} V_{\text{los,asc}} \\ V_{\text{los,dsc}} \\ V_{\text{azi,asc}} \\ V_{\text{azi,dsc}} \\ V_E^{\text{GPS}} \\ V_N^{\text{GPS}} \end{bmatrix} \tag{3}$$

Where $\theta_{\text{inc,asc}}$ and $\theta_{\text{inc,dsc}}$ Are the incidence angles for ascending and descending orbit. $\alpha_{\text{h,asc}}$ and $\alpha_{\text{h,dsc}}$ Are the satellite orbit headings for ascending and descending orbit. $V_{\text{los,asc}}$ and $V_{\text{los,dsc}}$ These are the deformation components of LOS for ascending and descending orbits. $V_{\text{azi,asc}}$ and $V_{\text{azi,dsc}}$ Are the azimuth offset components of the ascending and descending orbit. In radar geometry, the orbit heading indicates the direction of the satellite's trajectory. The heading value and the observation direction are different due to Sentinel-1's right-look angle orbit strategy (Brouwer and Hanssen 2024). In order to fix this, we refined the extracted heading values to create the azimuth look direction by following the research of Chang et al. (2018).

3 Result

3.1 DEM Accuracy Test Result

Every DEM utilized in this research has a unique vertical reference system. Copernicus and DEMNAS refer to the EGM2008 geoid vertical reference, where SRTM-1 refers to the EGM96 geoid model. The height reference system in relation to the WGS84 ellipsoid is used in field measurement data using the RTK method. The geoid undulation value (N) for each observation site in each DEM was used to convert geoid height to ellipsoid height using the following equation to align the vertical reference systems of each DEM and field measurement data (Wellenhof and Moritz 2005).

$$h = H + N \tag{4}$$

where h is the ellipsoidal height, H is the orthometric height, and N denotes the geoid undulation. The measurement results, with low RMS values, particularly in the horizontal component (0.002–0.012 m), show that the RTK approach has a high degree of precision. The readings stay within acceptable technical tolerance limits, even if the vertical precision (0.005–0.045 m) tends to be more varied. Furthermore, the consistently large number of satellites employed and the low PDOP values (ranging from 0.914 to 1.785) throughout the observations, which support spatial geometry stability, indicate an ideal satellite setup. It was verified that every field-measured observation point had a "fixed" solution status. This strengthens the validity of the measurement data, as it shows that the minimum accuracy and precision requirements were met during the measurement process (Furby and Akhavian 2024).

Table 2 Vertical accuracy calculation results

DEM	Mean (m)	$RMSE_z$ (m)	LE90 (m)
SRTM-1	3.873	1.968	3.247
Copernicus	3.450	1.857	3.065
DEMNAS	3.596	1.896	3.129

SRTM-1 has the highest mean (3.873 m), followed by DEMNAS (3.596 m) and Copernicus (3.450 m), according to the vertical accuracy results (Table 2). This demonstrates that Copernicus has the lowest vertical accuracy when compared to field measurements. The vertical value stability of each DEM is assessed using the RMSE metric. In this case, Copernicus has the lowest RMSE among the three DEMs, suggesting a more uniform error distribution. SRTM-1 has the highest RMSE, which may be due to greater elevation variations in the DEM. The LE90 of the three DEMs displays the most significant error at a 90% confidence level. Based on these results, Copernicus shows the best consistency and performance in accuracy when compared to the other two DEMs.

To ensure the best results and eliminate bias in calculation errors, this study conducted a series of statistical calculations on the distribution of Δh values in each DEM. This was done to determine whether the errors followed a normal distribution. The normality test used the Shapiro-Wilk test (Shapiro and Wilk 1965), which was chosen because it is proven to be more sensitive in detecting deviations from normal distribution in small sample sizes, where the number of points we calculated was 24. Other studies show that this approach is superior to other calculations in the context of limited data (DEMİR 2022; Noughabi 2018). Therefore, this method is the right choice to ensure the validity of the distribution assumption before conducting parametric or non-parametric tests in evaluating the vertical accuracy of DEM (Table 3). The results in Table 3 show that only Copernicus DEM does not show a normal distribution, while the other two DEMs have a normal distribution pattern. To maintain the validity of statistical calculations and avoid unmet distribution assumptions, a non-parametric approach was then applied.

Table 3 Shapiro–Wilk normality test results for DEM datasets

DEM	*p*-value	Distribution
DEMNAS	0.0960	Normal
Copernicus	0.0065	Non-normal
SRTM-1	0.9522	Normal

The error distribution in all DEMs did not meet the assumption of normality. This study used Repeated Measures ANOVA and then the Friedman test as a non-parametric alternative to compare DEM performance. Both methods work well for

evaluating DEMs at the same field points since they rank-pair data and do not require normality (Akar 2017). The analyses showed significant differences among the DEMs. To determine which pairs were significantly different, the Wilcoxon Signed-Rank test was employed as a post-hoc test (Chaikh et al. 2014). Even though the data were not normal, this test ranks DEM error differences (Chaikh et al. 2014).

Table 4 Wilcoxon signed-rank test pairwise comparison of DEM datasets

DEM pair	*p*-value	Interpretation
DEMNAS vs Copernicus	0.0047	Significant
DEMNAS vs SRTM-1	0.0026	Significant
Copernicus vs SRTM-1	0.4405	Not significant

It is evident from the computation values in Table 4 that DEMNAS has a significantly different error distribution from Copernicus and SRTM-1, whereas Copernicus and SRTM-1 do not have a significantly different distribution, indicating that there is no proof that the two have statistically different accuracy levels. Copernicus has the best vertical accuracy for the test points in the study region overall, according to the statistical test's combined findings. This is because the Wilcoxon Signed-Rank test between Copernicus and SRTM-1 has a P value of 0.4405, which is clearly above the statistical significance threshold. This indicates that there is no statistically significant difference between the two DEM models in terms of vertical error against field observation data. In other words, although numerically Copernicus shows a slightly lower RMSEz value than SRTM-1, DEMNAS has significant differences from the other two DEMs, with relatively lower performance based on the RMSE and LE90 values. Therefore, it can be concluded that Copernicus excels in terms of numbers in all accuracy parameters.

3.2 Analysis phase unwrapping DEM

An analysis of the unwrapping phase results for each different DEM was conducted to determine the extent of differences in topographic correction quality in the InSAR process. The parameters analyzed were the unwrapping success rate (in percent), topographic phase error range (rad/m), number of pixels formed, measurable deformation range along the LOS, and standard deviation (std) of DEM error. All calculation results are shown in Table 5.

In general, each DEM shows very competitive performance on both ascending and descending tracks. On the ascending track, Copernicus has the highest unwrapping percentage at 87.6%, slightly ahead of SRTM-1 and DEMNAS at 87.4% and 87.2%, respectively. On the descending path, Copernicus remains consistently superior to other DEMs with an unwrapping completion percentage of 83.5%, followed by SRTM-1 and DEMNAS. Based on the unwrapping percentage results, all three DEMs show good performance with a high success rate.

Table 5 Phase unwrapping analysis for each DEM and orbit direction

DEM	Parameter	Value
SRTM-1 (Asc)	Unwrapping percentage (%)	0.874
	DEM error (rad m^{-1})	−0.0129–0.0192
	Pixels	14,733
	LOS velocity (mm yr^{-1})	−6.003–7.087
	Std. DEM error	0.0034
Copernicus (Asc)	Unwrapping percentage (%)	0.876
	DEM error (rad m^{-1})	−0.0201–0.0683
	Pixels	14,754
	LOS velocity (mm yr^{-1})	−5.958–6.786
	Std. DEM error	0.0037
DEMNAS (Asc)	Unwrapping percentage (%)	0.872
	DEM error (rad m^{-1})	−0.0143–0.0197
	Pixels	14,709
	LOS velocity (mm yr^{-1})	−6.233–6.734
	Std. DEM error	0.0038
SRTM-1 (Dsc)	Unwrapping percentage (%)	0.833
	DEM error (rad m^{-1})	−0.0189–0.0796
	Pixels	29,074
	LOS velocity (mm yr^{-1})	−10.912–9.683
	Std. DEM error	0.0071
Copernicus (Dsc)	Unwrapping percentage (%)	0.835
	DEM error (rad m^{-1})	−0.0201–0.0683
	Pixels	30,202
	LOS velocity (mm yr^{-1})	−5.454–10.666
	Std. DEM error	0.0068
DEMNAS (Dsc)	Unwrapping percentage (%)	0.831
	DEM error (rad m^{-1})	−0.0679–0.0328
	Pixels	29,167
	LOS velocity (mm yr^{-1})	−7.310–10.062
	Std. DEM error	0.0064

DEM error demonstrates how bias in deformation estimations might result from DEM errors (Cigna et al. 2021). Poorly estimated deformations may arise from this kind of inaccuracy. To make sure there were no significant estimating mistakes in the estimated deformation data, an analysis was carried out. Copernicus displayed the largest margin of error on the climbing trajectory. This suggests that there will probably be more variations in topographic corrections. SRTM-1 and DEMNAS, on the other hand, seem to have substantially smaller ranges. The same pattern was seen on the descending trajectory, with DEMNAS once more displaying the largest margin of error. Copernicus and SRTM-1, on the other hand, typically fell within the same bounds and ranges.

There are roughly equal numbers of pixels examined from SAR data. The total number of pixels produced by all models is approximately 14,700 in ascending, with fewer than 50 pixels separating each model. The total of number using descending, Copernicus displayed the most pixels (30,202) on the descending track, followed

by SRTM-1 (29,074) and DEMNAS (29,167). In addition to indirectly reflecting the DEM's capacity to capture the local landscape, the number of pixels shows how well the unwrapping process went. The dynamics of deformation are displayed by the LOS deformation range (Fig. 3). On the ascending trajectory, the deformation rate ranges from −6.0 to 7.1 mm yr^{-1}. However, on the descending trajectory there is a sharper variation, with Copernicus showing the highest deformation range of −5.454 to 10.666 mm yr^{-1}, while DEMNAS shows a deformation range of −7.310 to 10.062 mm yr^{-1}, reflecting sensitivity in capturing more extreme ground movements in some areas. The distribution of observation pixels in the Ascending data shows significant limitations in the southeast region. Generated during processing, so the color representation is the result of spatial interpolation by the software. Therefore, this region is excluded from the deformation interpretation because it does not meet the interferometric validation criteria.

In this study, statistical indicators for evaluating the stability of topographic corrections in InSAR processing were examined based on the standard deviation of DEM error (Uss et al. 2020). The ascending trajectory shows that SRTM-1 has the smallest standard deviation, followed by Copernicus and DEMNAS. Although the difference in standard deviation for each DEM is relatively small, this order shows that the most consistent topographic correction on the ascending trajectory is using the SRTM-1 DEM. In the context of DEM deformation, this provides consistent topographic correction and is also sensitive to small phase variation changes. Conversely, on the descending trajectory, DEMNAS has the smallest standard deviation when compared to Copernicus DEM and SRTM-1. However, this small difference in standard deviation is not enough to indicate which DEM is the most consistent across all analysis parameters. When assessed as a whole, Copernicus DEM excels on both ascending and descending trajectories

3.3 Azimuth Tracking Offset

This study retrieved amplitude values from the range and azimuth domains of Sentinel–1 data to examine the initial indicators of backscatter signal stability and ground surface roughness. We chose a few scenes to examine persistent reflectance patterns over the course of the observation time from a total of 150 scenes and 76 scenes of Sentinel-1 ascending and descending track data. This amplitude distribution is representative enough to demonstrate the stability of radar texture between times and between pathways, even though only a small piece of the complete dataset is shown. This forms the basis for selecting image pairs for azimuth offset estimation, with priority given to areas that show consistent reflectivity and minimal temporal disturbance. The presence of recurring reflective features also reinforces the potential application of sub-pixel accuracy (Sartika et al. 2023) and accurate spatial correlation at the offset tracking stage (Du et al. 2022; Peng et al. 2022). In this study, we used SBAS logic to calculate the azimuth offset for each pair (Huang et al. 2020). Thus, the number of azimuth offset pairs is equal to the number of SBAS method pairs to obtain LOS velocity. The main difficulty in performing the azimuth tracking azimuth offset method in this study was the extreme movement we obtained due to high noise. This occurred because of the poor azimuth resolution of Sentinel-1 and the small amount

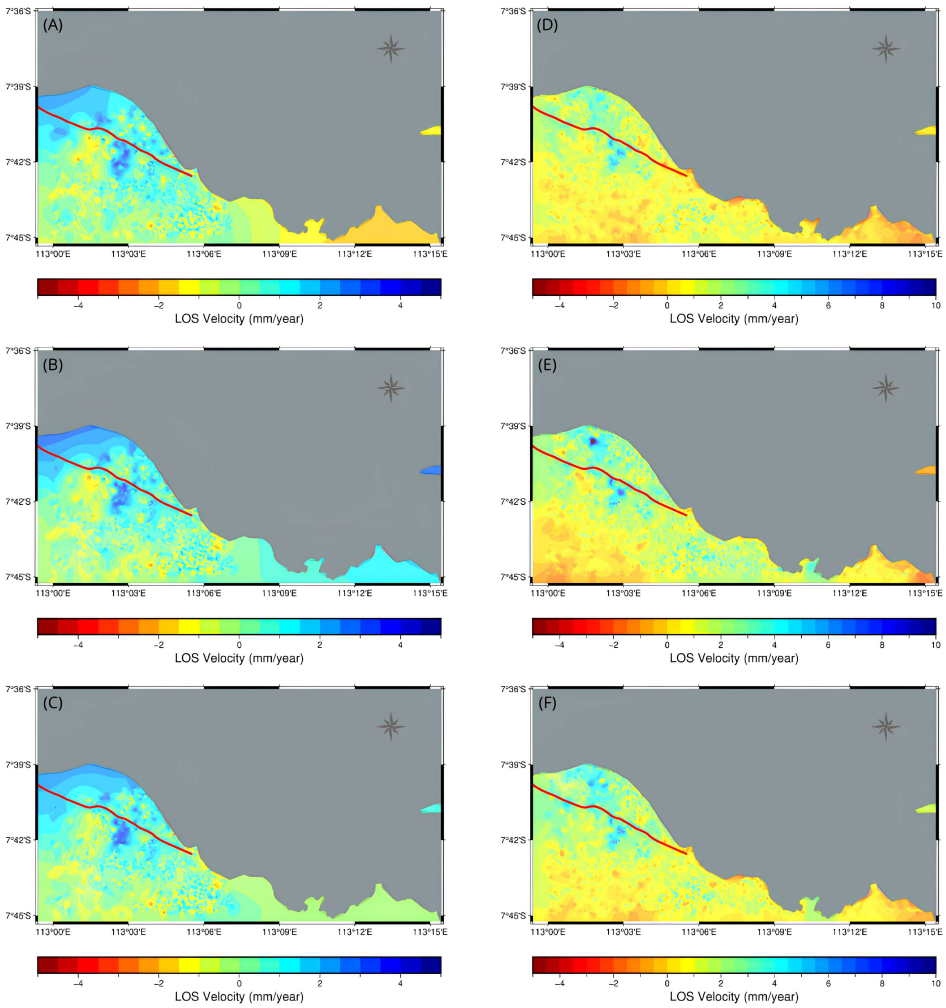


Fig. 3 LOS velocity of Sentinel-1 data study area, ascending (A-C) and descending (D-F) tracks.

of fault movement and fault deformation recorded in both LOS InSAR and Ina-CORS station observations.

3.4 Decomposition Result

In the decomposition process, this study performed calculations based on the creation of points with a grid size of 10 x 10 meters. Thus, 1,533,310 points were formed in the study area. To calculate the decomposition of the three components (VU, VE, and VN), the values of each parameter resulting from the processing of ascending and descending LOS InSAR, azimuth tracking offset, and also the Ina-CORS GPS components (Ve and Vn). For the horizontal component from the Ina-CORS GPS station, we are using local velocity calculations that were carried out for each observation

station point, which were carried out by Maulida et al. (2023). Other parameters in performing the decomposition require heading and incidence angle in the ascending and descending directions (Dai et al. 2022; Chang et al. 2018) (Fig. 4).

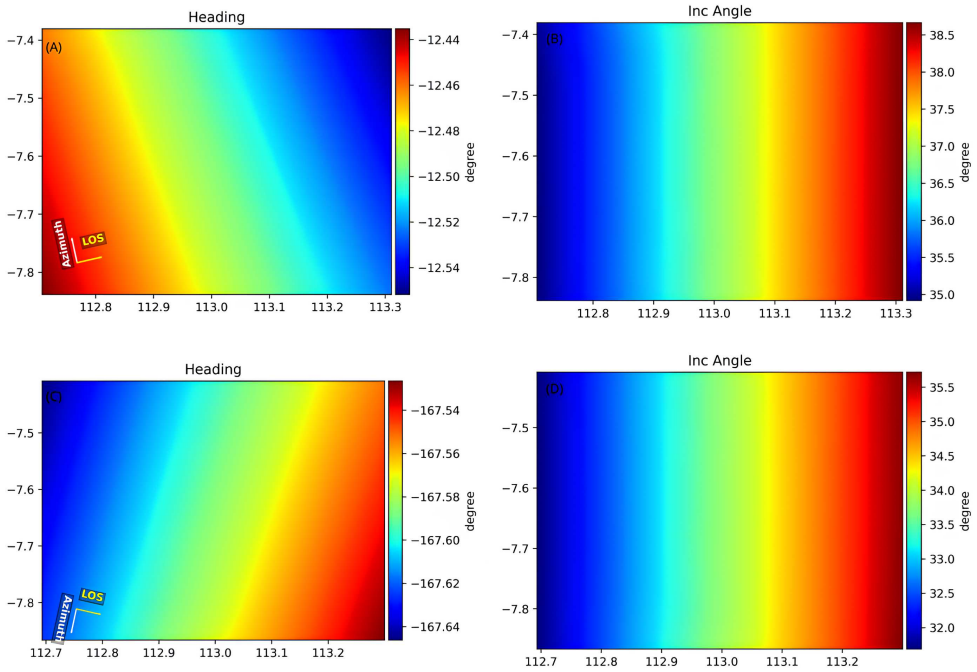


Fig. 4 The Heading and Incidence angle data of Sentinel-1 in the study area. (A–B) Heading and Incidence angle Ascending and (C–D) Heading and Incidence angle Descending.

The decomposition process produced three surface deformation velocity components: VU, VE, and VN, which are shown in Fig. 5. Results are given by means of LOS InSAR data, azimuth tracking offset, and GPS station Ina-CORS components Ve and Vn according to Equation 3. The method is rooted in the decomposition approach given by Hayati et al. (2023) and Zhou et al. (2021), where a system of linear equations calculates each velocity component.

VU represents the vertical component, which shows the subsidence or uplift displacement. It is associated with the Pasuruan normal fault plane. The horizontal components of VE and VN show horizontal displacement in the study area. These findings are supported by previous studies, such as Marliyani et al. (2019), which reported tectonic activity in the East Java backarc zone. The observed range for Ve is around 5.09 mm/year on the southwest side to 4.06 mm/year in the northeast part. There is an evident west-to-east trend in the pattern. The red line marks the pattern of the changes in the horizontal movement of blocks near the fault. For the Vn component, about 2.78 mm/year on the west side and about 2.27 mm/year on the east side are

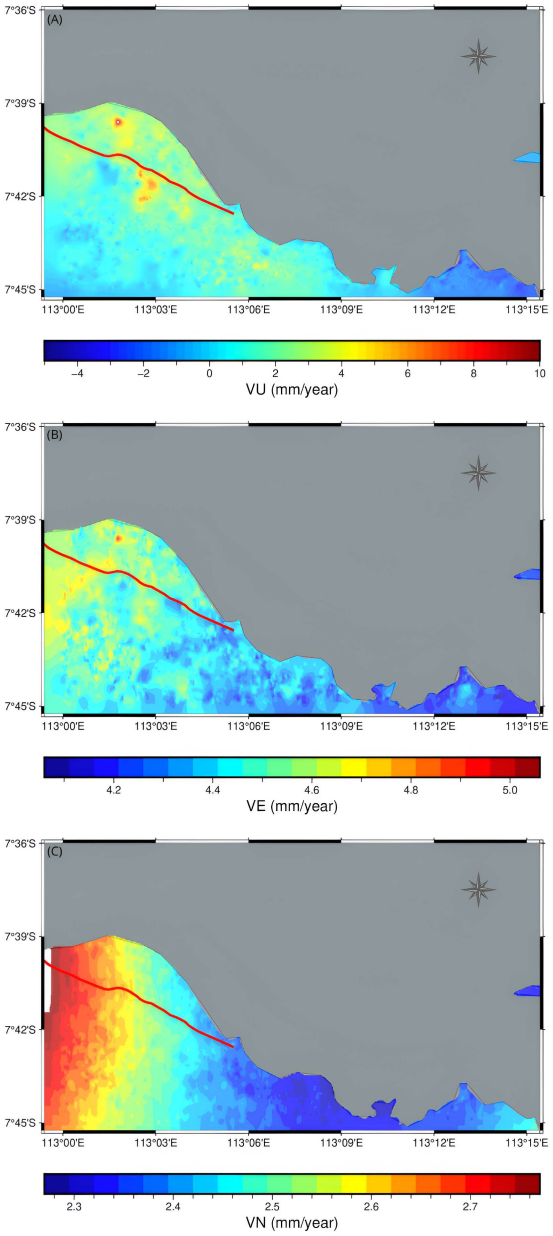


Fig. 5 Visualization of interpolated velocity components resulting from decomposition. (A) V_U (vertical); (B) V_E (east–west); (C) V_N (north–south).

observed. Opposite north-south deformation between blocks fits this pattern, according to Fialko and Simons (2001). Such a difference in velocity manifests as a horizontal strain gradient around the fault, with one block moving slightly faster northward than the other (Marliyani et al. 2019).

4 Discussions

4.1 External evaluation of DEM phase unwrapping accuracy

Different sources of vertical accuracy results indicate that Copernicus DEM performs best, according to this study. A DEM plays a crucial role in the InSAR processing chain, primarily because it removes the topographic component from the interferogram before unwrapping. Errors in the DEM will leave phase residues, making the unwrapping far more challenging and affecting the deformation estimates. High quality DEMs are shown by Hanssen (2001) and Ducret et al. (2013) for unwrapping, especially in complex terrain.

Liu et al. (2023) reported that Copernicus should be used to obtain InSAR data in a mainly flat area, as it produces fewer surface artifacts that can confuse the results. The current research supports this, demonstrating that the Copernicus DEM has the highest vertical accuracy. The accuracy of a DEM also depends on the moment of the acquisition and the spatial resolution. Using a recent DEM is a good way to avoid phase errors caused by surface changes, as it better represents the current Earth (Torun et al. 2023).

The differentiation in unwrapping accuracy closely depends on the decision of the DEMs and their quality, which has been confirmed by Torun et al. (2023). They found that the root mean square error (RMSE) is lower in areas with gentle slopes and higher in those with steep slopes. Though DEMNAS has higher spatial resolution, it still performs poorly in terms of accuracy and phase unwrapping. This study states that the right choice of DEM can improve deformation accuracy by reducing bias and errors. Removing DEM issues and ensuring vertical accuracy can facilitate processing and reduce DEM errors (Liang et al. 2019). The present study's use of the Copernicus DEM is consistent with previous work and highlights the importance of high-quality DEMs in SAR-based deformation studies.

4.2 Azimuth Tracking offset in the Decomposition equation

With some restrictions, the azimuth-tracking offset approach in this study can identify shifts or deformations along the azimuth direction. This method uses a Gaussian fit for sub-pixel refining and an NCC approach for Sentinel-1 amplitude. To increase the signal-to-noise ratio without sacrificing sensitivity, a 64x64 pixel window size was used (Du et al. 2022). In an attempt to capture shifts in the study region, we adjusted the offset search range in the azimuth direction to 2 pixels, or s $\pm$40 meters, based on the Sentinel-1 azimuth pixel resolution. The correlation threshold we used was 0.3 to filter out insignificant matching results. We realize that this threshold value is the lowest threshold compared to similar studies. Our data processing experience shows that many pixels are lost when we use a threshold of 0.45 (Hu et al. 2014).

Another approach we took was sub-pixel accuracy to obtain a better azimuth offset by considering the minimal deformation that can be recorded with this method in the study area (Hu et al. 2014). However, we normalized the trend calculation results by setting a velocity threshold of ±50 mm/yr, thereby eliminating values that were larger or smaller than this. We realize that eliminating these azimuth velocity values makes our results unrepresentative of the actual azimuth movement, but we did so because of the large bias and noise that would occur if we did not. Therefore, this method must continue to be developed and computational improvements made to obtain results that are truly representative in observing the deformation that occurs along the SAR azimuth direction.

4.3 Analysis of Decomposition Results

Evaluation of decomposition results by combining LOS InSAR results (combining PS-InSAR and SBAS), azimuth tracking offset, and GPS data from the Ina-CORS station through Pearson correlation analysis. The correlation analysis emphasized in this study is the decomposition results of the horizontal components (VE and VN) compared with the vn and ve components from the Ina-CORS GPS station, and the correlation between the vertical components (VU) of the decomposition results and LOS InSAR on the ascending and descending trajectories.

Fig. 6 shows a plot indicating that the velocity of the VE and VN component decomposition has a very good correlation with the velocity of the component from the GPS station, with a correlation value of r = 0.995 with RMSE 0.013 and r = 0.842 with RMSE 0.081. This component shows that the decomposition results are able to capture the movement patterns occurring in the east-west and north-south directions quite well and consistently with the GPS station measurement results. The decomposition results of this component can adequately represent deformation and fault movement analysis. This is also explained in the study by Hamdi et al. (2023) that the integration of GPS observations and InSAR results can produce horizontal accuracy in the range of mm/year.

The VE component, representing another aspect of the horizontal decomposition (Fig. 6A), demonstrates a strong correlation with GPS data, with a correlation coefficient of r = 0.995. This finding indicates that integrating multiple parameters in the decomposition is effective for detecting north-south movements. The calculation model applied in this study yields accurate projections and inversions in this direction. Environmental factors such as vegetation and difficult terrain are not really reasons one cannot capture the VN component. However, a high correlation does not necessarily mean that the error will be low at every observation point. Low coherence or steep slopes can still lead to inaccurate deformation estimates. Hence, it is reasonable to assess data quality and deformation status before deciding to combine GPS and InSAR for decomposition calculations (Shen and Liu 2020). The reason for this consideration is that the GPS data from the Ina-CORS station are interpolated and a very sparse distribution of CORS stations (Fig. 7) (Béjar-pizarro et al. 2016), as there is no Ina-CORS GPS station near the study area.

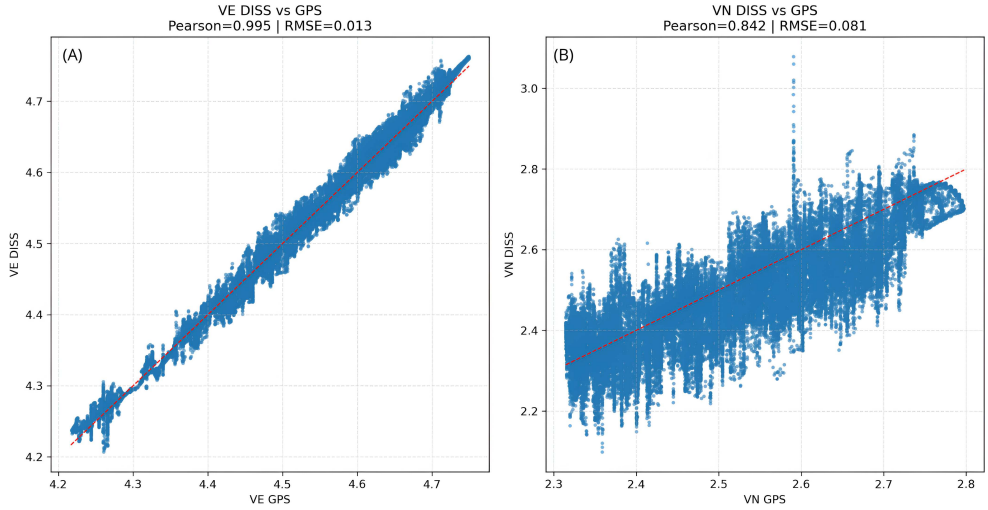


Fig. 6 Pearson correlation between the horizontal components of the decomposition results (DISS) and the GPS components of the Ina-CORS station. (A) GPS Ve component with VE decomposition results, (B) GPS Vn component with VN decomposition results.

The line-of-sight (LOS) InSAR decomposition just using ascending and descending paths is highly consistent with the vertical component (VU) obtained from the decomposition analysis (Fig. 8). The ascending and descending track is associated with the VU component at r = 1.000 with RMSE 0.01. Each path has different sensitivities to vertical movement, but the point distributions of both tracks show that they are suitable for vertical estimation. The variations in azimuth could also cause differences in the look angle and incidence angle for each track (Dai et al. 2022). Using both ascending and descending tracks in SAR data processing (Liu et al. 2020), along with the fusion of PS-InSAR and SBAS techniques, is more effective for determining the vertical component than either a single track or a single InSAR method (Fikri et al. 2024).

This study also aims to highlight the correlation between the vertical component of the Ina-CORS station's GPS (Vu) and the VU component resulting from decomposition, as shown in Fig. 9. This is necessary to justify the correlation between the vertical shift component resulting from decomposition and the LOS InSAR results and the vertical component resulting from GPS observations at the Ina-CORS station. The correlation shown in this comparison has an r = 0.50. The correlation of the GPS vertical component with the decomposition result VU is lower when compared to the vertical component compared with the LOS result. This also shows that the interpolation results for the vertical component from Ina-CORS do not represent actual vertical motion in the area of study. So, for the vertical component, we use the overall results of the InSAR decomposition on ascending and descending.

Considering the correlation results discussed above, there are several important points in this study. By combining the LOS InSAR results with the PS-InSAR and SBAS methods on two tracks, azimuth tracking offset, and the Ina-CORS GPS station, this study was able to represent a much higher density of deformation observation

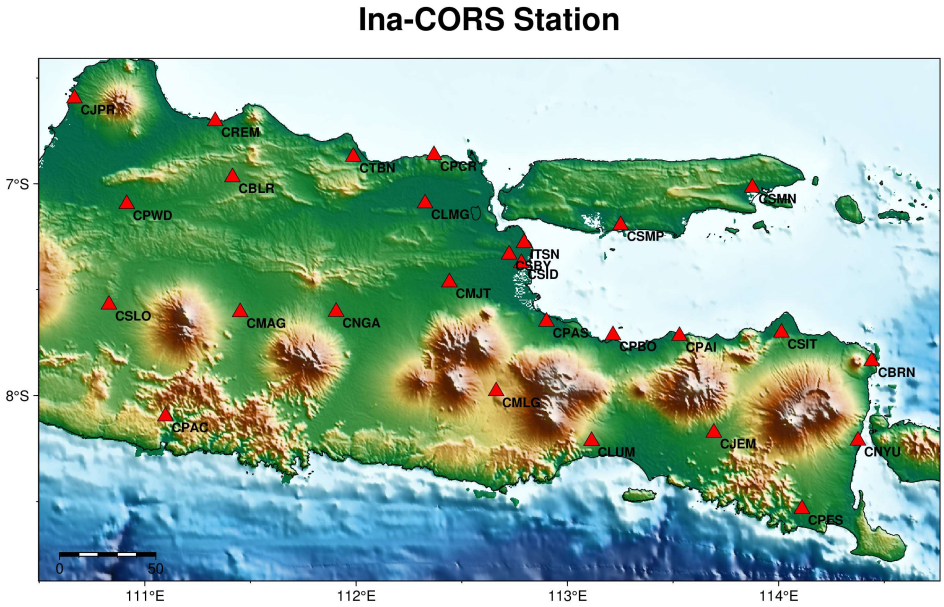


Fig. 7 Distribution of GPS points at the Ina-CORS Station in East Java.

points compared to GPS data alone. Although the correlation in the vertical component is quite good when compared to the LOS InSAR results on both tracks, there is still a greater margin of uncertainty compared to the horizontal component. This factor is a methodological limitation in this study. Validation of GPS campaign observations is key in further research to analyze the deformation occurring on the Pasuruan fault. Although several components show high correlations that reinforce the excellent decomposition results, other studies show that GPS remains a comparative reference in decomposing InSAR and GPS observations to obtain high accuracy (Alonso-Díaz et al. 2025).

4.4 Analysis of Decomposition with Java Tectonics

The component resulting from decomposition, we use to analyze with another research that explains tectonics on the island of Java. We model the result of horizontal decomposition to analyze the direction of movement that occurs (Fig. 10). The horizontal velocity decomposition results shown in Fig. 10 indicate a dominant northwest (NW) movement pattern at the study site. This direction is consistent with the oblique convergence mechanism reported by previous studies. Koulali et al. (2017) identified, through block deformation modeling in Java, that the southern segment of East Java experienced northwestward movement relative to the Sunda block, in response to the subduction of the Indo-Australian Plate beneath Eurasia. Similarly, Maulida et al. (2023), using Ina-CORS GPS data for the 2017?2022 period, showed that the velocity vector at the same location pointed NW.

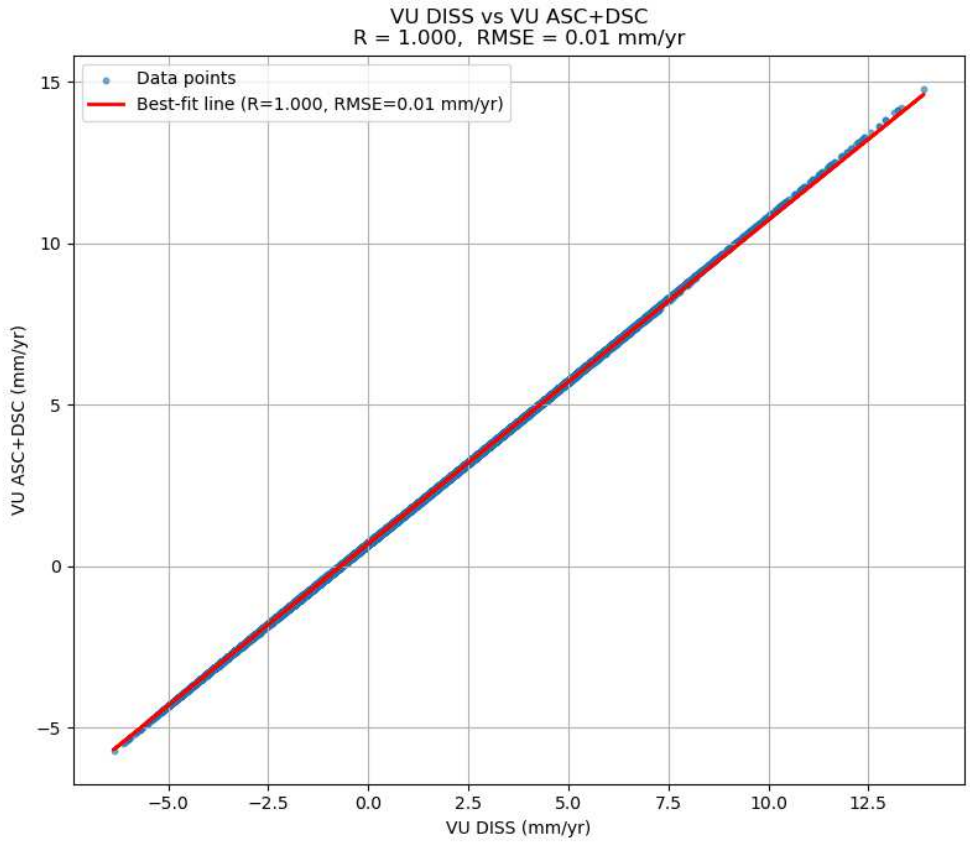


Fig. 8 Vertical (VU) component from decomposition of this research correlation with decomposition using LOS InSAR ascending and descending to compute VU component.

Overall, the agreement between the movement directions of this study and previous studies (Koulali et al. 2017; Maulida et al. 2023) validates the applied decomposition approach. This confirms that the East Java region, particularly the Pasuruan fault region, is part of the Sunda oblique deformation system that has the potential to generate large earthquakes, both from subduction zones and onshore faults in the back-arc. Therefore, continuous monitoring using GPS and integration with InSAR is crucial for updating hazard models in this region.

5 Conclusions

This study reinforces the importance of multi-data and multi-method integration in analyzing deformation in fault zones in a geodetic context, and places the decomposition results as a good quantitative basis for further analysis. Analysis of the vertical accuracy of DEMs from various sources shows that Copernicus DEM excels in all

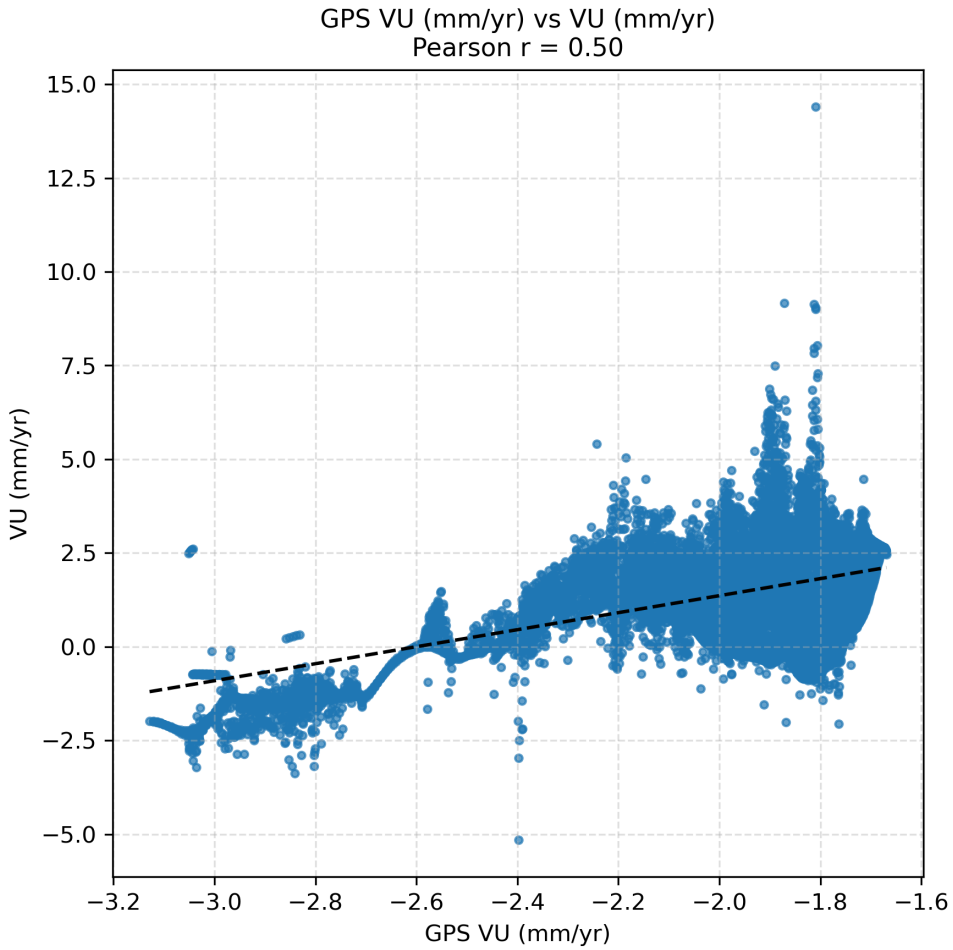


Fig. 9 Correlation of the vertical component of the GPS Ina-COS Station (Vu) with the vertical component (VU) resulting from the decomposition.

aspects. In terms of accuracy, this DEM is better than the other two DEMs, SRTM-1 and DEMNAS. This is because the DEM is able to display a representation of the actual surface elevation in the study area (Liu et al. 2023). In the InSAR processing, the Copernicus DEM also showed the best performance in terms of unwrapping success rate, DEM error (rad/m), number of pixels formed, and standard deviation of DEM error. Knowing the best DEM to use will certainly improve the accuracy of deformation mapping (Torun et al. 2023). Thus, the formation of the decomposition calculation will eliminate errors resulting from InSAR processing.

Based on the decomposition analysis developed in this study, based on previous studies, there are several important notes that must be reconsidered. Although the success of the decomposition in this study shows a good correlation and the results of

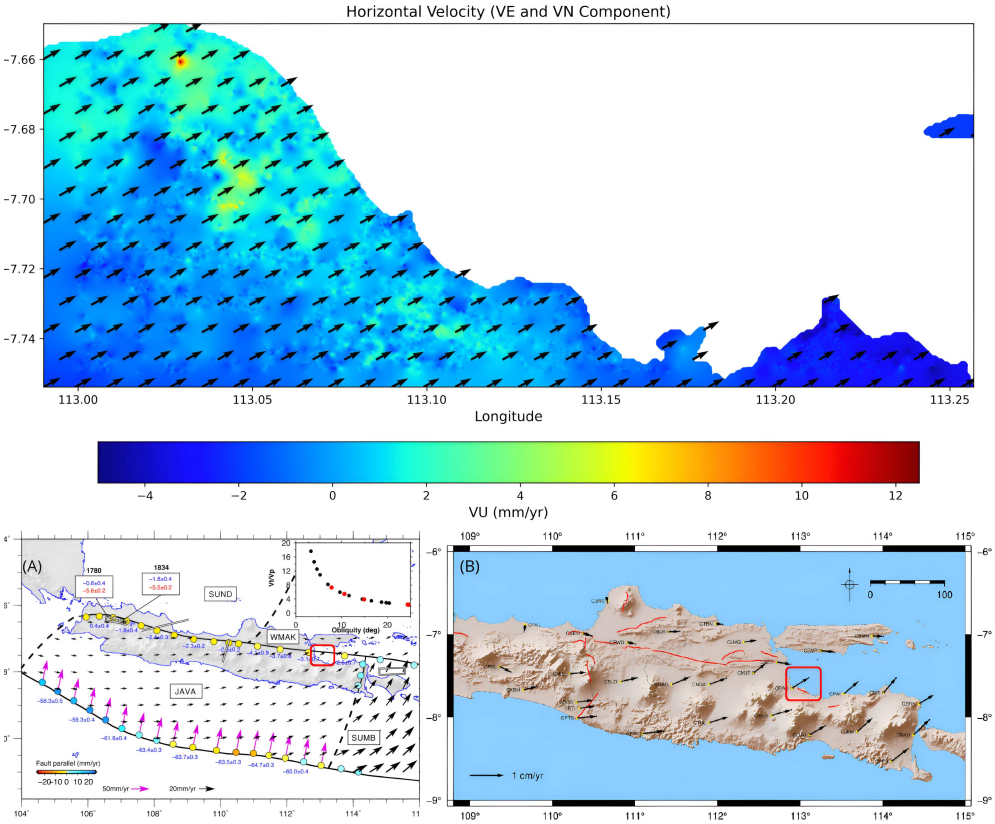


Fig. 10 Horizontal velocity based on decomposition results. (A) Block modeling of the Java region (Koulali et al. 2017) and (B) Velocity Sunda block from the GPS Ina-CORS station in Java (Maulida et al. 2023).

the tectonic analysis of this decomposition component are in line with existing tectonic research, there are still some irregularities that need to be investigated further. One of them is the development of the azimuth tracking offset method. In this study, the researchers adaptively provided certain limitations in data processing, as explained in the previous sub-chapter. This resulted in the azimuth tracking offset results being unable to represent the azimuth shift well. However, this effect does not significantly affect the decomposition results, so the decomposition model is still very good when viewed from the calculation results.

Not only the azimuth tracking offset method, but this study also highlights the interpolation results of all components generated by the Ina-CORS station GPS observation (Maulida et al. 2023). Limitations with a fairly wide distribution and the absence of Ina-CORS stations within the research area indicate that the observation results from GPS components are not representative when viewed from the interpolation results (Béjar-pizarro et al. 2016). Further research involves conducting periodic GPS campaigns to obtain the best results. Thus, the decomposition results can be used in geodetic strain and slip analysis in the Pasuruan fault zone.

Acknowledgements. This research was supported by the Ministry of Higher Education, Science, and Technology of the Republic of Indonesia under the Doctoral Research Scheme. The authors acknowledge the European Space Agency for providing Sentinel-1 SAR data and the Geospatial Information Agency of Indonesia (BIG) for providing DEMNAS data. The authors also thank the developers of StaMPS and ISCE for making their software publicly available.

Author contributions. SF and IMA: conceptualization and study design; SF, IMA, and PM: methodology and data processing; SF and MN: validation; SF and IMA: formal analysis; SF and PM: software development; SF: investigation; IMA: resources and supervision; SF, IMA, and MN: manuscript preparation and original draft; SF and IMA: manuscript review and editing.

Declarations

- Funding
  This research was supported by the Ministry of Higher Education, Science, and Technology of the Republic of Indonesia through the BIMA Program, Dissertation Research Grant (PDD) scheme Grant Number: 017/C3/DT.05.00/PL/2025
- Availability of data and materials
  All digital elevation model (DEM) datasets used in this study are openly available in public repositories. The Copernicus DEM (30 m resolution) is available from the Copernicus Space Component Data Access portal (accessed 9 May 2025). The SRTM-1 DEM is available from the United States Geological Survey (USGS) Land Processes Distributed Active Archive Center (LP DAAC) (accessed 6 March 2025). The DEMNAS dataset is available from the Geospatial Information Agency of Indonesia (BIG) through the national geospatial data portal (accessed 12 April 2024).
- Declaration of generative AI and AI-assisted technologies in the manuscript preparation process
  During the preparation of this manuscript, the authors used Grammarly to improve the clarity and structure of the writing. After using this tool, the authors reviewed and edited the content as necessary and take full responsibility for the content of the published article.
- Competing interests
  The authors declare no competing interests.

References

Alonso-Díaz, A., Solla, M., Bakon, M., Sousa, J.: Improvement associated with mesh geometry for the decomposition of InSAR results. Geo-Spatial Information Science **00**(00), 1–19 (2025) https://doi.org/10.1080/10095020.2025.2547948

Airbus Defence and Space: Copernicus Digital Elevation Model - Product Handbook, pp. 1–36 (2022)

Akar, A.: Evaluation of Accuracy of Dems Obtained From Uav-Point Clouds for Different Topographical Areas. International Journal of Engineering and Geosciences **2**(3), 110–117 (2017) https://doi.org/10.26833/ijeg.329717

Badan Informasi Geospasial: DEMNAS (2018). https://tanahair.indonesia.go.id/demnas/{#}/

Badan Standarisasi Nasional: Standar Nasional Indonesia Ketelitian Peta Dasar (2019)

Berardino, P., Fornaro, G., Lanari, R., Sansosti, E.: A new algorithm for surface deformation monitoring based on small baseline differential SAR interferograms. IEEE Trans. Geosci. Remote. Sens. **40**(11), 2375–2383 (2002) https://doi.org/10.1109/TGRS.2002.803792

Brouwer, W.S., Hanssen, R.F.: Estimating three-dimensional displacements with InSAR: the strapdown approach. Journal of Geodesy **98**(12), 1–15 (2024) https://doi.org/10.1007/s00190-024-01918-2

Bouraoui, S.: Time series analysis of SAR images using persistent scatterer (PS), small baseline (SB) and merged approaches in regions with small surface deformation Seyfallah Bouraoui To cite this version : Présentée à L ' Université de Strasbourg pour l ' obtenti. PhD thesis, Université de Strasbourg (2013)

Béjar-pizarro, M., Guardiola-Albert, C., García-cárdenas, R.P., Staller, A., Ortega-Becerril, J.A., García-García, R.P., Herrera, G., Barra, A., Molina, A.L., Tessitore, S., Staller, A., Ortega-Becerril, J.A., García-García, R.P.: Interpolation of GPS and geological data using InSAR deformation maps: Method and application to land subsidence in the alto guadalentín aquifer (SE Spain). Remote Sensing **8**(11) (2016) https://doi.org/10.3390/rs8110965

Bayer, B., Schmidt, D., Simoni, A.: The influence of external digital elevation models on PS-InSAR and SBAS results: Implications for the analysis of deformation signals caused by slow moving landslides in the northern apennines (Italy). IEEE Transactions on Geoscience and Remote Sensing **55**(5), 2618–2631 (2017) https://doi.org/10.1109/TGRS.2017.2648885

Chang, L., Dollevoet, R.P.B.J., Hanssen, R.F.: Monitoring Line-Infrastructure with Multisensor SAR Interferometry: Products and Performance Assessment Metrics. IEEE Journal of Selected Topics in Applied Earth Observations and Remote Sensing **11**(5), 1593–1605 (2018) https://doi.org/10.1109/JSTARS.2018.2803074

Chaikh, A., Giraud, J.Y., Perrin, E., Bresciani, J.P., Balosso, J.: The choice of statistical methods for comparisons of dosimetric data in radiotherapy. Radiation Oncology **9**(1), 1–11 (2014) https://doi.org/10.1186/1748-717X-9-205

Clements, B., Hall, R., Smyth, H.R., Cottam, M.A.: Thrusting of a volcanic arc: A

new structural model for Java. Petroleum Geoscience **15**(2), 159–174 (2009) https://doi.org/10.1144/1354-079309-831

Chae, S.H., Lee, W.J., Baek, W.K., Jung, H.S.: An Improvement of the Performance of SAR Offset Tracking Approach to Measure Optimal Surface Displacements. IEEE Access **7**, 131627–131637 (2019) https://doi.org/10.1109/ACCESS.2019.2938831

Cigna, F., Ramírez, R.E., Tapete, D.: Accuracy of sentinel-1 PSI and SBAS InSAR displacement velocities against GNSS and geodetic leveling monitoring data. Remote Sensing **13**(23), 1–28 (2021) https://doi.org/10.3390/rs13234800

Dabove, P., Di Pietra, V.: Single-baseline RTK positioning using dual-frequency GNSS receivers inside smartphones. Sensors (Switzerland) **19**(19) (2019) https://doi.org/10.3390/s19194302

Ducret, G., Doin, M.P., Grandin, R., Lasserre, C., Guillaso, S.: DEM corrections before unwrapping in a small baseline strategy for InSAR time series analysis. IEEE Geoscience and Remote Sensing Letters **11**(3), 696–700 (2013) https://doi.org/10.1109/LGRS.2013.2276040

DEMİR, S.: Comparison of Normality Tests in Terms of Sample Sizes under Different Skewness and Kurtosis Coefficients. International Journal of Assessment Tools in Education **9**(2), 397–409 (2022) https://doi.org/10.21449/ijate.1101295

Dai, K., Feng, Y., Zhuo, G., Tie, Y., Deng, J., Balz, T., Li, Z.: Applicability Analysis of Potential Landslide Identification by InSAR in Alpine-Canyon Terrain - Case Study on Yalong River. IEEE Journal of Selected Topics in Applied Earth Observations and Remote Sensing **15**, 10131–10139 (2022) https://doi.org/10.1109/JSTARS.2022.3228948

Du, S., Mallorqui, J.J., Zhao, F.: Patch-Like Reduction (PLR): A SAR Offset Tracking amplitude filter for deformation monitoring. International Journal of Applied Earth Observation and Geoinformation **113**(January), 102976 (2022) https://doi.org/10.1016/j.jag.2022.102976

Furby, B., Akhavian, R.: A Comprehensive Comparison of Photogrammetric and RTK-GPS Methods for General Order Land Surveying. Buildings **14**(6) (2024) https://doi.org/10.3390/buildings14061863

Fikri, S., Anjasmara, I.M., Cahyadi, M.N.: Integration of PS-InSAR and SBAS Methods with Different DEM for Monitoring the Activity of the Kendeng Fault in the Surabaya and Waru Segments. 2024 IEEE Asia-Pacific Conference on Geoscience, Electronics and Remote Sensing Technology (AGERS), 305–310 (2024) https://doi.org/10.1109/AGERS65212.2024.10932962

Farr, T.G., Kobrick, M.: Shuttle radar topography mission produces a wealth of data. Eos **81**(48), 583–585 (2000) https://doi.org/10.1029/EO081i048p00583

Ferretti, A., Prati, C., Rocca, F.: Permanent scatterers in SAR interferometry. IEEE Transactions on Geoscience and Remote Sensing **39**(1), 8–20 (2001) https://doi.org/10.1109/36.898661

Fialko, Y., Simons, M.: The complete (3-D) surface displacement field in the epicentral area of the 1999 M7.1 Hector Mine earthquake California from space geodetic observations. Geophysical Research Letters **28**(16), 3063–3066 (2001)

Fang, L., Ye, Z., Su, S., Kang, J., Tong, X.: Glacier surface motion estimation from sar intensity images based on subpixel gradient correlation. Sensors (Switzerland) **20**(16), 1–18 (2020) https://doi.org/10.3390/s20164396

Guth, P.L., Van Niekerk, A., Grohmann, C.H., Muller, J.P., Hawker, L., Florinsky, I.V., Gesch, D., Reuter, H.I., Herrera-Cruz, V., Riazanoff, S., López-Vázquez, C., Carabajal, C.C., Albinet, C., Strobl, P.: Digital elevation models: Terminology and definitions. Remote Sensing **13**(18), 1–19 (2021) https://doi.org/10.3390/rs13183581

Hanssen, R.F.: Radar Interferometry: Data Interpretation and Error Analysis. Remote Sensing and Digital Image Processing. Springer, Dordrecht (2001). https://doi.org/10.1007/0-306-47633-9

Huang, J., Bai, Y., Lei, S., Deng, K.: Time-Series SBAS Pixel Offset Tracking Method for Monitoring Three-Dimensional Deformation in a Mining Area. IEEE Access **8**, 118787–118798 (2020) https://doi.org/10.1109/ACCESS.2020.3004460

Hamdi, L., Defaflia, N., Merghadi, A., Fehdi, C., Yunus, A.P., Dou, J., Pham, Q.B., Abdo, H.G., Almohamad, H., Al-Mutiry, M.: Ground Surface Deformation Analysis Integrating InSAR and GPS Data in the Karstic Terrain of Cheria Basin, Algeria. Remote Sensing **15**(6) (2023) https://doi.org/10.3390/rs15061486

Hussain, E., Hooper, A., Wright, T.J., Walters, R.J., Bekaert, D.P.S.: Interseismic strain accumulation across the central North Anatolian Fault from iteratively unwrapped InSAR measurements. Journal of Geophysical Research: Solid Earth **121**(12), 9000–9019 (2016) https://doi.org/10.1002/2016JB013108

Hayati, N., Niemeier, W., Maulida, P., Bioresita, F., Nuryani, H.W.: A Computation to Generate 2D and 3D Vector Displacements Using InSAR Ascending and Descending Source Data (Case Studies: Landslides and Earthquake in Indonesia). Indonesian Journal on Geoscience **10**(3), 323–334 (2023) https://doi.org/10.17014/ijog.10.3.323-334

Hooper, A.: A multi-temporal InSAR method incorporating both persistent scatterer and small baseline approaches. Geophysical Research Letters **35** (2008) https://doi.org/10.1029/2008GL034654

Hu, X., Wang, T., Liao, M.: Measuring coseismic displacements with point-like targets

offset tracking. IEEE Geoscience and Remote Sensing Letters **11**(1), 283–287 (2014) https://doi.org/10.1109/LGRS.2013.2256104

Jiang, M., Guarnieri, A.M.: Distributed Scatterer Interferometry with the Refinement of Spatiotemporal Coherence. IEEE Transactions on Geoscience and Remote Sensing **58**(6), 3977–3987 (2020) https://doi.org/10.1109/TGRS.2019.2960007

Julzarika, A., Harintaka: Indonesian DEMNAS: DSM or DTM? AGERS 2019 - 2nd IEEE Asia-Pacific Conference on Geoscience, Electronics and Remote Sensing Technology: Understanding and Forecasting the Dynamics of Land, Ocean and Maritime, Proceeding, 31–36 (2019) https://doi.org/10.1109/AGERS48446.2019.9034351

Koulali, A., McClusky, S., Susilo, S., Leonard, Y., Cummins, P., Tregoning, P., Meilano, I., Efendi, J., Wijanarto, A.B.: The kinematics of crustal deformation in Java from GPS observations: Implications for fault slip partitioning. Earth and Planetary Science Letters **458**, 69–79 (2017) https://doi.org/10.1016/j.epsl.2016.10.039

Liang, H., Member, S.S., Zhang, L., Member, S.S., Lu, Z., Li, X.: Nonparametric estimation of DEM error in multitemporal in SAR. IEEE Transactions on Geoscience and Remote Sensing **57**(12), 10004–10014 (2019) https://doi.org/10.1109/TGRS.2019.2930802

Liu, Z., Wang, T.: High-Resolution Interseismic Strain Mapping From InSAR Phase-Gradient Stacking: Application to the North Anatolian Fault With Implications for the Non-Uniform Strain Distribution Related to Coseismic Slip Distribution. Geophysical Research Letters **50**(15) (2023) https://doi.org/10.1029/2023GL104168

Liu, L., Yu, J., Chen, B., Wang, Y.: Urban subsidence monitoring by SBAS-InSAR technique with multi-platform SAR images: a case study of Beijing Plain, China. European Journal of Remote Sensing **53**(sup1), 141–153 (2020) https://doi.org/10.1080/22797254.2020.1728582

Liu, H., Zhou, B., Bai, Z., Zhao, W., Zhu, M., Zheng, K., Yang, S., Li, G.: Applicability Assessment of Multi-Source DEM-Assisted InSAR Deformation Monitoring Considering Two Topographical Features. Land **12**(7) (2023) https://doi.org/10.3390/land12071284

Marliyani, G.I., Arrowsmith, J.R., Helmi, H.: Evidence for Multiple Ground-Rupturing Earthquakes in the Past 4,000 Years Along the Pasuruan Fault, East Java, Indonesia: Documentation of Active Normal Faulting in the Javan Backarc. Tectonics **38**(4), 1489–1506 (2019) https://doi.org/10.1029/2018TC005255

Ma, P., Huang, C., Hou, J., Zhang, Y., Han, W., Dou, P.: Snow Depth Retrieval With Multiazimuth and Multisatellite Data Fusion of GNSS-IR Considering the Influence of Surface Fluctuation. IEEE Transactions on Geoscience and Remote Sensing **61**, 1–14 (2023) https://doi.org/10.1109/TGRS.2023.3323642

Maulida, P., Rafiq, M., Herawati, Y.A., Kurniawan, A., Taufik, M.: Current deformation in eastern part of Java derived from GPS observation 2017-2022. IOP Conference Series: Earth and Environmental Science **1276**(1), 0–12 (2023) https://doi.org/10.1088/1755-1315/1276/1/012023

Noughabi, H.A.: A Comprehensive Study on Power of Tests for Normality. Journal of Statistical Theory and Applications **17**(4), 647 (2018) https://doi.org/10.2991/jsta.2018.17.4.7

Purwaningsih, R.E.Y., Sekarsari, A., Sari, T.W., Pratama, C., Wibowo, S.T.: Active tectonics of the eastern java based on a decade of recent continuous geodetic observation. Geodesy and Geodynamics **13**(4), 376–385 (2022) https://doi.org/10.1016/j.geog.2021.12.004

Peng, L., Wang, H., Ng, A.H.M., Yang, X.: SAR Offset Tracking Based on Feature Points. Frontiers in Earth Science **9**(February), 1–10 (2022) https://doi.org/10.3389/feart.2021.724965

Qin, Y., Perissin, D., Bai, J.: Investigations on the coregistration of Sentinel-1 TOPS with the conventional cross-correlation technique. Remote Sensing **10**(9), 1–23 (2018) https://doi.org/10.3390/rs10091405

Sartika, S., Brahmantara, R.P., Rahayu, M.I., Candra, D.S., Hestrio, Y.F., Ulfa, K., Prabowo, Y., Novresiandi, D.A., Veronica, K.W.: A Sub-pixel Geometric Evaluation for Very High-Resolution Satellite Images using Phase Cross-Correlation Algorithm. In: AIP Conference Proceedings, vol. 2941 (2023). https://doi.org/10.1063/5.0181398

Sartika, M., Jaya, L.M.G., Nurgiantoro, N.: Pemetaan Sebaran Total Suspended Solid (TSS) dan Khlorofil-a (chl-a) pada Perairan Sungai Wanggu menggunakan Citra Sentinel-2. Jurnal Geografi Aplikasi dan Teknologi **3**(2), 49–56 (2019)

Shen, Z.K., Liu, Z.: Integration of GPS and InSAR Data for Resolving 3-Dimensional Crustal Deformation. Earth and Space Science **7**(4) (2020) https://doi.org/10.1029/2019EA001036

Susetyo, D.B.: Vertical Accuracy Assessment of Various Open-Source Dem Data: Demnas, Srtm-1, and Aster Gdem. Geodesy and Cartography (Vilnius) **49**(4), 209–215 (2023) https://doi.org/10.3846/gac.2023.18168

Shapiro, S.S., Wilk, M.B.: An Analysis of Variance Test for Normality (Complete Samples). Biometrika **52**(3/4), 591 (1965) https://doi.org/10.2307/2333709

Torun, A.T., Ekercin, S., Algancı, U., Yılmaztürk, F.: Evaluating the Effect of External DEMs on the Accuracy of InSAR DEM Generation. Journal of the Indian Society of Remote Sensing **51**(1), 213–225 (2023) https://doi.org/10.1007/s12524-022-01640-6

Uss, M.L., Vozel, B., Lukin, V.V., Chehdi, K.: Estimation of Variance and Spatial Correlation Width for Fine-Scale Measurement Error in Digital Elevation Model. IEEE Transactions on Geoscience and Remote Sensing **58**(3), 1941–1956 (2020) https://doi.org/10.1109/TGRS.2019.2951178

Wellenhof, B.H., Moritz, H.: Physical Geodesy, Second edi edn., p. 403. Springer, ??? (2005). https://books.google.co.id/books?id=71VfLRmplg4C

Wright, T.J., Parsons, B.E., Lu, Z.: Toward mapping surface deformation in three dimensions using InSAR. Geophysical Research Letters **31**(1), 1–5 (2004) https://doi.org/10.1029/2003GL018827

Widjajanti, N., Pratama, C., Parseno, Sunantyo, T.A., Heliani, L.S., Ma'ruf, B., Atunggal, D., Lestari, D., Ulinnuha, H., Pinasti, A., Ummi, R.F.: Present-day crustal deformation revealed active tectonics in Yogyakarta, Indonesia inferred from GPS observations. Geodesy and Geodynamics **11**(2), 135–142 (2020) https://doi.org/10.1016/j.geog.2020.02.001

Weiss, J.R., Walters, R.J., Morishita, Y., Wright, T.J., Lazecky, M., Wang, H., Hussain, E., Hooper, A.J., Elliott, J.R., Rollins, C., Yu, C., González, P.J., Spaans, K., Li, Z., Parsons, B.: High-Resolution Surface Velocities and Strain for Anatolia From Sentinel-1 InSAR and GNSS Data. Geophysical Research Letters **47**(17) (2020) https://doi.org/10.1029/2020GL087376

Yan, L., Xiong, Q., Li, D., Cheon, E., She, X., Yang, S.: InSAR-Driven Dynamic Landslide Hazard Mapping in Highly Vegetated Area. Remote Sensing **16**(17) (2024) https://doi.org/10.3390/rs16173229

Zhang, P., Qian, X., Guo, S., Wang, B., Xia, J., Zheng, X.: A New Method for Continuous Track Monitoring in Regions of Differential Land Subsidence Rate Using the Integration of PS-InSAR and SBAS-InSAR. Remote Sensing **15**(13) (2023) https://doi.org/10.3390/rs15133298

Zhou, W., Zhang, W., Yang, X., Wu, W.: An Improved GNSS and InSAR Fusion Method for Monitoring the 3D Deformation of a Mining Area. IEEE Access **9**, 155839–155850 (2021) https://doi.org/10.1109/ACCESS.2021.3129521